

# Brane universes tested against astronomical data

Mariusz P. Dąbrowski\*

*Institute of Physics, University of Szczecin, Wielkopolska 15, 70-451 Szczecin, Poland*

Włodzimierz Godłowski<sup>†</sup> and Marek Szydłowski<sup>‡</sup>

*Astronomical Observatory, Jagiellonian University, 30-244 Krakow, ul. Orla 171, Poland*

(Dated: January 4, 2019)

We discuss observational constraints coming from supernovae imposed on the behaviour of the Randall-Sundrum models. We test the models using the Perlmutter SN Ia data as well as the new Knop and Tonry/Barris samples. The data indicates that, under the assumption that we admit zero pressure dust matter on the brane, the cosmological constant is still needed to explain current observations. We estimate the model parameters using the best-fitting procedure and the likelihood method. The observations from supernovae give a large value of the density parameter for brane matter  $\Omega_{\lambda,0} \simeq 0.01$  as the best fit. For high redshifts  $z > 1.2$ , the difference between the brane model and the  $\Lambda$ CDM (Perlmutter) model becomes detectable observationally. From the maximum likelihood method we obtained the favored value of  $\Omega_{\lambda,0} = 0.004 \pm 0.016$  for  $\Omega_{k,0} = 0$  and  $\Omega_{m,0} = 0.3$ . This gives the limit  $\Omega_{\lambda,0} < 0.02$  at  $1\sigma$  level. While the model with brane effects is preferred by the supernovae type Ia data, the model without brane fluid is still statistically admissible. We also discuss how fit depends on restrictions of the sample, especially with respect to redshift criteria. We also pointed out the property of sensitive dependence of results with respect to choice of  $\mathcal{M}$  parameter. For comparison the limit on brane effects which comes from CMB anisotropies and BBN is also obtained. The uncertainty in the location of the first peak gives a stronger limit  $\Omega_{\lambda,0} < 1.0 \cdot 10^{-12}$ , whereas from BBN we obtain that  $\Omega_{\lambda,0} < 1.0 \cdot 10^{-27}$ . However, both very strict limits are obtained with the assumption that brane effects do not change the physics in the pre-recombination era, while the SN Ia limit is model independent.

We demonstrate that the fit to supernovae data can also be obtained if we admit the phantom matter  $p = -(4/3)\rho$  on the brane, where this matter mimics the influence of the cosmological constant. We show that phantom matter enlarges the age of the universe on the brane which is demanded in cosmology. Finally, we propose to check for dark radiation and brane tension by the application of the angular diameter of galaxies minimum value test.

PACS numbers: 04.20.Jb,04.65.+e,98.80.Hw

## I. INTRODUCTION

The idea of brane universes has originated from Hořava and Witten [1] followed by Randall and Sundrum [2]. In the Randall-Sundrum scenarios of the brane-world cosmology the large extra dimensions can solve the mass hierarchy problem of the standard model. In this model the basic cosmological equations are modified by the presence of some extra terms which are derived from the fact that our universe is treated as a three-brane - to which all the gauge interactions are confined - embedded in a five-dimensional, anti-de Sitter space, in (the whole of) which only gravity can propagate. The cosmological evolution of such brane universes has been extensively investigated [2, 3, 4, 5, 6] (for a review see [7]). For example, the issues related to the cosmological constant problem [8], the cosmological perturbations [9, 10], inflationary solutions [11], homogeneity, and flatness problems [12, 13] were discussed.

Brane models admit new parameters which are not present in standard cosmology (brane tension  $\lambda$  and dark radiation  $\mathcal{U}$ ). From the astronomical observations of supernovae Ia [14, 15, 16, 17, 18, 19] one knows that the universe is now accelerating and the best-fit model is for the 4-dimensional cosmological constant density parameter  $\Omega_{\Lambda_4,0} = 0.72$  and for the dust density parameter  $\Omega_{m,0} = 0.28$  (index "0" refers to the present moment of time). In other words, only the exotic (negative pressure) matter in standard cosmology can lead to this global effect. On the other hand, in brane models the  $\rho^2$  quadratic contribution in the energy density  $\rho$  even for a small negative pressure, contributes effectively as the positive pressure, and makes brane models less accelerating. In this paper we argue that in order to avoid this problem one requires much stronger negative pressure  $p < -\rho$  (phantom) matter to be present on the brane (cf. Ref. [20, 21]).

We concentrate on some observational constraints on the  $\rho^2$  term, which depending on the type of matter present scales with the cosmic scale factor as  $a^{-6\gamma}$ , where  $\gamma$  is the barotropic index in the equation of state  $p = (\gamma - 1)\rho$  ( $p$  - the pressure and  $\rho$  - the energy density). In fact, the  $\rho^2$  term scales as  $a^{-6}$  (similarly as stiff-fluid in standard cosmology) for dust  $\gamma = 1$  matter, as  $a^{-8}$  for radiation  $\gamma = 4/3$  and as  $a^2$  for phantom

\*Electronic address: mpdabfz@uoo.univ.szczecin.pl

<sup>†</sup>Electronic address: godlows@oa.uj.edu.pl

<sup>‡</sup>Electronic address: uoszydlo@cyf-kr.edu.pl

matter  $\gamma = -1/3$ .

In this paper we discuss the observational constraints imposed on the brane-world cosmologies by supernovae type Ia observations. Preliminary results of such analysis were made in [32]. Since we do not know how the exotic physics of brane theory works in the early stages of the Universe (for example, during structure formation), then all estimations of the brane influence onto the Cosmic Microwave Background (CMB) and Big Bang Nucleosynthesis (BBN) are based on the assumption that this exotic physics does not change physical processes afterwards. The advantage of SNIa data is its independence of the physical processes in the early universe. Therefore, despite the fact that weaker limits from SNIa observations can be obtained, they are in this sense more valuable. We demonstrate that the brane model fits the SN Ia data very well. We also show that these observations indicate a substantial contribution from the brane, although the observational constraints from BBN and CMB restrict this contribution to a much higher degree. However, to derive the limits from BBN and CMB we assume that brane effects did not change physics before the recombination epoch. On the other hand, the less restrictive limit we obtained from SN Ia data is not so strongly dependent on the assumptions of a model.

We argue that the admission of the brane effects for the dust matter on the brane does not fit supernovae data without the presence of the cosmological constant, but we can avoid this problem if we admit phantom matter on the brane. Also, we argue that in the near future, when new supernovae data is available (SNAP3), the hypothesis of important brane effects at present ( $\Omega_{\lambda,0} > 0$ ) will be tested.

In Section II we present the basic equations of brane cosmology which are studied dynamically in Section III. Sections IV and V are devoted to a redshift-magnitude relation for brane universes and its comparison with supernovae type Ia data. In Section VI we discuss the angular diameter size of a galaxy for brane universes together with the age of the universe problem. In Section VII we obtain the restrictions onto the brane universes from the observations of the Doppler peaks in CMB while in Section VIII we give the restrictions which come from BBN. In Section IX we give our conclusions.

## II. BASIC EQUATIONS OF BRANE COSMOLOGY

Hořava and Witten [1] and Randall and Sundrum [2] provided us with an alternative mechanism of compactification of extra dimensions which is different from the conventional Kaluza-Klein scheme because extra dimensions are segments (called orbifolds) rather than compact spaces like the circle. Based on the Randall-Sundrum brane model we can derive the effective 4-dimensional Einstein equations by projecting 5-dimensional metric onto the brane world-volume. The dynamics of brane

models is obtained from the 5-dimensional Einstein equations with brane location at  $y = 0$  as [3]

$${}^{(5)}\tilde{G}_{\mu\nu} = \kappa_5^2[-\Lambda_5^{(5)}g_{\mu\nu} + \delta(y)(-\lambda^{(4)}h_{\mu\nu} + {}^{(4)}T_{\mu\nu})] , \quad (1)$$

where  ${}^{(5)}\tilde{G}_{\mu\nu}$  is the 5-dimensional Einstein tensor,  ${}^{(5)}g_{\mu\nu}$  is the 5-dimensional metric,  $y$  is an orbifold coordinate,  $\Lambda_5$  is the 5-dimensional cosmological constant,  ${}^{(4)}h_{\mu\nu} = {}^{(5)}g_{\mu\nu} - n_\mu n_\nu$  is 4-dimensional induced metric,  $n^\alpha$  is the unit vector normal to the brane,  ${}^{(4)}T_{\mu\nu}$  is the 4-dimensional energy-momentum tensor,  $\lambda$  is the brane tension, and  $\kappa_5^2 = 8\pi^{(5)}G_N = 8\pi/{}^{(5)}M_p^3$  is the 5-dimensional Einstein constant. The main point is that the 5-dimensional Planck mass can be much less from the 4-dimensional Planck mass  ${}^{(5)}M_p \ll {}^{(4)}M_p = 1.2 \cdot 10^{19}\text{GeV}$  and so the electroweak scale  ${}^{(5)}M_p \sim \text{TeV}$  may be reached in the Earth accelerators.

The 4-dimensional Einstein equations on the brane are

$${}^{(5)}G_{\mu\nu} = -\Lambda_4^{(4)}h_{\mu\nu} + \kappa_4^2 + \kappa_5^2\Pi_{\mu\nu} - E_{\mu\nu} , \quad (2)$$

where

$$\kappa_4^2 = 8\pi^{(4)}G_N = \frac{8\pi}{{}^{(4)}M_p^2} = \kappa_5^4 \frac{\lambda}{6} , \quad (3)$$

$$\Lambda_4 = \frac{1}{2}\kappa_5^2 \left( \Lambda_5 + \frac{1}{6}\kappa_5^2\lambda^2 \right) , \quad (4)$$

$$\Pi_{\mu\nu} = \frac{1}{12}TT_{\mu\nu} - \frac{1}{4}T_{\mu\alpha}T_\nu^\alpha + \frac{1}{24}g_{\mu\nu}[3T_{\alpha\beta}T^{\alpha\beta} - T^2] \quad (5)$$

where  $\Lambda_4$  the 4-dimensional cosmological constant and  $\kappa_4^2 = 8\pi G = 8\pi \times 10^{-38}(\text{GeV})^{-2}$  is the 4-dimensional Einstein constant. For the homogeneous and isotropic Friedmann models the Einstein field equations reduce to a generalized Raychaudhuri equation [3]

$$\dot{H} = -H^2 - \frac{1}{6}\kappa_4^2 \left[ \rho + 3p + (2\rho + 3p)\frac{\rho}{\lambda} \right] + \frac{\Lambda_4}{4} - \frac{2\mathcal{U}}{\lambda\kappa_4^2} \quad (6)$$

where the dark radiation  $\mathcal{U}$  results from the Weyl tensor contribution to 5-dimensional geometry which is related to the fact of non-vanishing of the energy-momentum tensor of matter on the brane. The dark radiation obeys the conservation law

$$\dot{\mathcal{U}} = -4H\mathcal{U} . \quad (7)$$

The conservation law for matter in the form of perfect fluid is

$$\dot{\rho} = -3(\rho + p)H , \quad (8)$$

which for barotropic fluid gives

$$\dot{\rho} = -3\gamma H\rho , \quad (9)$$

and shows that the conservation law for equation (7) is simply the conservation law for radiation ( $\gamma = 4/3$ ), except  $\mathcal{U}$  can take on both positive and negative values.

In Ref. [23] we gave the formalism to express dynamical equations in terms of dimensionless observational density parameters  $\Omega$ . Following Refs. [24, 25, 26] we introduce the notation useful for this purpose. In this notation the Friedmann equation for brane universes takes the form which is the first integral of Equations (6)–(8)

$$H^2 = \frac{\kappa_{(4)}^2}{3}\rho + \frac{\kappa_{(4)}^2}{6\lambda}\rho^2 - \frac{k}{a^2} + \frac{\Lambda_4}{3} + \frac{2\mathcal{U}}{\lambda\kappa_{(4)}^2}, \quad (10)$$

where  $a(t)$  is the scale factor,  $k = 0, \pm 1$  the curvature index. After imposing conservation law (9) we have

$$\rho a^{3\gamma} = \text{const.} \quad (11)$$

which brings the Eq. (10) to the form

$$\frac{1}{a^2} \left( \frac{da}{dt} \right)^2 = \frac{C_{GR}}{a^{3\gamma}} + \frac{C_\lambda}{a^{6\gamma}} - \frac{k}{a^2} + \frac{\Lambda_4}{3} + \frac{C_U}{a^4}. \quad (12)$$

In Eq. (12) we have defined the appropriate constants  $C_{GR} = (1/3)\kappa_{(4)}^2 a^{3\gamma}\rho$ ,  $C_\lambda = 1/6\lambda \cdot \kappa_{(4)}^2 a^{6\gamma}\rho^2$ ,  $C_U = 2/\kappa_{(4)}^2 \lambda \cdot a^4 \mathcal{U}$ , and  $C_{GR}$  is a of general relativistic nature,  $C_\lambda$  comes as contribution from brane tension  $\lambda$ , and  $C_U$  as a contribution from dark radiation. Though in Refs. [23, 27] the Eq. (12) was studied using qualitative methods we briefly discuss here the cases  $\gamma = 0$  (cosmological constant),  $\gamma = 1/3$  (domain walls) and  $\gamma = 2/3$  (cosmic strings) which can exactly be integrable in terms of elementary or elliptic [24] functions.

The first case  $\gamma = 0$  is the easiest, since the first two terms on the right-hand-side of (12) play the role of cosmological constants similar to  $\Lambda_4$

$$\frac{1}{a^2} \left( \frac{da}{dt} \right)^2 = \left( C_{GR} + C_\lambda + \frac{\Lambda_4}{3} \right) - \frac{k}{a^2} + \frac{C_U}{a^4}. \quad (13)$$

The next two cases involve terms which were already integrated in the context of general relativity. For  $\gamma = 1/3$  (domain walls on the brane) the general relativistic term  $C_{GR}$  in (12) scales as domain walls in general relativity while the term with  $C_\lambda$  scales as cosmic strings (curvature) in general relativity, i.e.,

$$\frac{1}{a^2} \left( \frac{da}{dt} \right)^2 = \frac{C_\lambda - k}{a^2} + \frac{C_{GR}}{a} + \frac{\Lambda_4}{3} + \frac{C_U}{a^4}. \quad (14)$$

For  $\gamma = 2/3$  (cosmic strings) the general relativistic term  $C_{GR}$  in (12) scales as cosmic strings in general relativity, while the term with  $C_\lambda$  scales as radiation in general relativity (compare [28, 44]), i.e.,

$$\frac{1}{a^2} \left( \frac{da}{dt} \right)^2 = \frac{C_U + C_\lambda}{a^4} + \frac{C_{GR} - k}{a^2} + \frac{\Lambda_4}{3}, \quad (15)$$

with an effective curvature index  $k' \equiv k - C_{GR}$ . Then, the problem of writing down exact solutions, which are elementary, reduces to the repetition of the discussion of

Ref. [24]. We will not be doing this here. For other values of  $\gamma = 4/3; 1; 2$  the terms of the type  $1/a^8$  and  $1/a^{12}$  appear, and the integration involves hyperelliptic integrals.

Let us also consider the case of  $\gamma = -1/3$  (phantom) [20], i.e.,

$$\frac{1}{a^2} \left( \frac{da}{dt} \right)^2 = C_{GR}a + C_\lambda a^2 - \frac{k}{a^2} + \frac{C_U}{a^4} + \frac{\Lambda_4}{3}. \quad (16)$$

A simple general relativistic solution for which  $C_\lambda = C_U = \Lambda_4 = 0$ ,  $C_{GR} \equiv C_{ph}$ ,  $k = 0$  (flat models) reads as

$$1/a(t) = \frac{1}{4} C_{ph} (t - t_0)^2. \quad (17)$$

However, it is more interesting to consider a spatially closed universe with  $k = +1$  which reads as

$$a(t) = \sqrt{\frac{-1}{C_{ph}^{\frac{1}{2}} \sin 2(t - t_0)}}. \quad (18)$$

This immediately shows that the admissible domain for time is:  $\pi/2 \leq (t - t_0) \leq \pi$ . It is interesting to notice that in (18) both initial (Big-Bang) and final (Big-Crunch) singularities emerge for infinite values of the scale factor (i.e.,  $\rho \rightarrow \infty$  when  $a(t) \rightarrow \infty$ ). This is because  $\rho = C_{ph} a$  in a conservation law. The new type of singularities are now commonly called Big-Rip singularities [20, 21].

It is easy to verify that the standard FRW limit can be obtained from (10) by taking  $1/\lambda \rightarrow 0$ , i.e., where the inverse of the brane tension tends to zero. The contribution from the brane  $\rho^2$  term is important only when  $\rho > \lambda > (100\text{GeV})^4$ .

The type of cosmology we study (cf. Eq. (10)) is a special case of a generalized brane model which is now commonly called a Cardassian model [29, 30]. In the Cardassian model the second term on the right-hand side of the equation (10) has an arbitrary power  $n$  of the energy density. For brane models we study  $n = 2$ .

In order to study observational tests we now define dimensionless observational density parameters [25, 26]

$$\begin{aligned} \Omega_{GR} &= \frac{\kappa_{(4)}^2}{3H^2}\rho, & \Omega_\lambda &= \frac{\kappa_{(4)}^2}{6H^2\lambda}\rho^2, & \Omega_U &= \frac{2}{\kappa_{(4)}^2 H^2\lambda}\mathcal{U}, \\ \Omega_k &= -\frac{k}{H^2 a^2}, & \Omega_{\Lambda_4} &= \frac{\Lambda_{(4)}}{3H^2}, \end{aligned} \quad (19)$$

where the Hubble parameter  $H = \dot{a}/a$ , and the deceleration parameter  $q = -\ddot{a}a/\dot{a}^2$ , so that the Friedmann equation (12) can be written down in the form

$$\Omega_{GR} + \Omega_\lambda + \Omega_k + \Omega_{\Lambda_{(4)}} + \Omega_U = 1. \quad (20)$$

Note that  $\Omega_U$  in (19), despite standard radiation term, can either be positive or negative. Using (19), the equation (12) can also be rewritten as (compare Eq.(10) of [25])

$$\Omega_{\Lambda_4} = \frac{3\gamma - 2}{2}\Omega_{GR} + (3\gamma - 1)\Omega_\lambda + \Omega_U - q. \quad (21)$$

It is also useful to express the curvature of spatial sections in terms of observational parameters by using (20) and (21)

$$-\Omega_k = \frac{3\gamma}{2}\Omega_{GR} + 3\gamma\Omega_\lambda + 2\Omega_{\mathcal{U}} - q - 1. \quad (22)$$

These relations (21) and (22) may allow to write down observational quantities for the brane models to study their compatibility with astronomical data which is the main objective of the present paper. Obviously, these quantities depend on the present densities of the different components of matter content  $\Omega$  given by (19) and their equations of state reflected by the value of the barotropic index  $\gamma$ .

### III. BRANE MODELS IN A TWO-DIMENSIONAL PHASE PLANE

For the considerations of this section and without the loss of generality it is useful to simplify the equation (10) by assuming that the parameters  $\kappa_4^2 = 1$  and  ${}^4M_p^2 = 8\pi$  which gives

$$\lambda = \frac{6}{\kappa_5^4}, \quad \Lambda_4 = \frac{1}{2}\sqrt{\frac{6}{\lambda}}\Lambda_5 + \frac{1}{2}\lambda,$$

so that the equation (10) reads as

$$H^2 = \frac{\rho}{3} \left(1 + \frac{\rho}{2\lambda}\right) + \frac{1}{6} \left(\sqrt{\frac{6}{\lambda}}\Lambda_5 + \lambda\right) - \frac{k}{a^2} + \frac{2\mathcal{U}_0}{\lambda a^4}, \quad (23)$$

and it contains only three independent constant  $\lambda$ ,  $\Lambda_5$  and  $\mathcal{U}_0$ . The last constant comes from the conservation law of dark radiation (7). Without losing a generality in our subsequent analysis we also put  $\Lambda_5 = 1$  so that the equation (23) takes the form

$$H^2 = \frac{\rho}{3} + \frac{\rho^2}{6\lambda} + \frac{\Lambda_4}{3} - \frac{k}{a^2} + \frac{\mathcal{C}_{\mathcal{U}}}{a^4}. \quad (24)$$

As we have mentioned already brane cosmology with the Randall-Sundrum ansatz is mathematically equivalent to a multifluid Friedmann cosmology. It is governed by the following dynamical system [23]

$$\begin{aligned} \dot{x} &= y, \\ \dot{y} &= -\frac{\partial V}{\partial x} = -\frac{1}{2} \sum_i \Omega_{i,0} (3\gamma_i - 2) x^{-(3\gamma_i-1)}, \end{aligned} \quad (25)$$

where dot denotes differentiation with respect to a new rescaled time variable  $T: t \rightarrow T \equiv |H_0|t$ ; and  $\Omega_{i,0}$  are the density parameters as defined in (19);  $x = a/a_0$ , and  $p_i = (\gamma_i - 1)\rho_i$ . For the sake of this Section we choose that a 4-dimensional brane universe is filled with *non-relativistic* matter (dust) *on the brane* only and the cosmological constant, so that we effectively put  $\gamma_m = 1$ ,  $\gamma_\lambda = 2$  (this is due to the fact that dust contribution

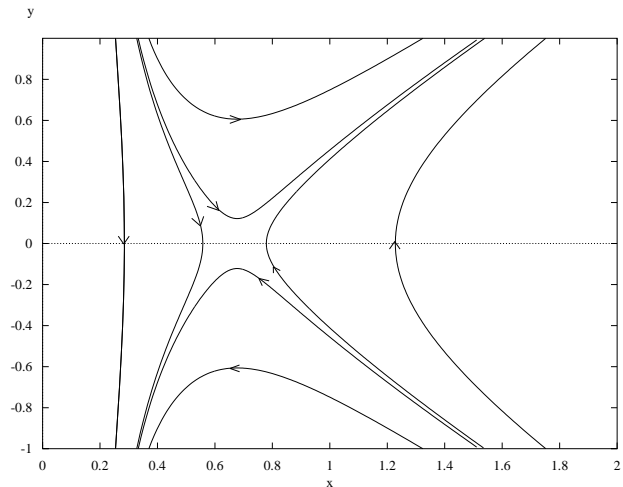


FIG. 1: The phase portrait of the system (25). There is one critical point – a saddle point. This critical point  $(x_0, 0)$  represents the Einstein Static Universe. The accelerating models lie in the domain  $x > x_0$ . Therefore the acceleration region is situated to the right of the saddle point. The flat model trajectory  $\Omega_{k,0} = 0$  separates the regions of the models with negative curvature  $\Omega_{k,0} > 0$  and positive curvature  $\Omega_{k,0} < 0$ . The line  $x = 1$  corresponds to  $a = a_0$ .

which comes from non-relativistic matter scales as stiff-fluid in standard case - cf. eqs. (11)-(12),  $\gamma_\Lambda = 0$ . However, as we already mentioned, the brane ( $\rho^2$ ) contribution from other types of fluids will scale differently simulating various types of fluids in standard cosmology.

Here,  $V(x)$  plays the role of the potential function for the system (25)

$$V(x) = -\frac{1}{2} \left( \Omega_{k,0} + \sum_i \Omega_{i,0} x^{-(3\gamma_i-2)} \right). \quad (26)$$

Let us note that the dynamics can also be represented in terms of a Hamiltonian dynamical system with the Hamiltonian of the form

$$\mathcal{H} = \frac{p_x^2}{2} + V(x),$$

and the system should be considered on the zero-energy level

$$\mathcal{H} = 0. \quad (27)$$

The phase portrait of the system (25) for the case of the dust  $\gamma = 1$  matter on the brane with  $\Omega_{\Lambda,0} = 0.69$ ,  $\Omega_{m,0} = 0.3$ ,  $\Omega_{\lambda,0} = 0.01$  is demonstrated in Fig. 1.

The differences in the behavior of trajectories manifest at high densities. Then, the structure of the dynamical behavior at infinity is modified. In order to illustrate the behavior of trajectories at infinity, the system (25) is represented in Fig. 2 in the projective coordinates

$$z = \frac{1}{x}, \quad u = \frac{y}{x}, \quad (z, u) - \text{map} \quad (28)$$

$$v = \frac{1}{y}, \quad w = \frac{x}{y}, \quad (v, w) - \text{map}. \quad (29)$$

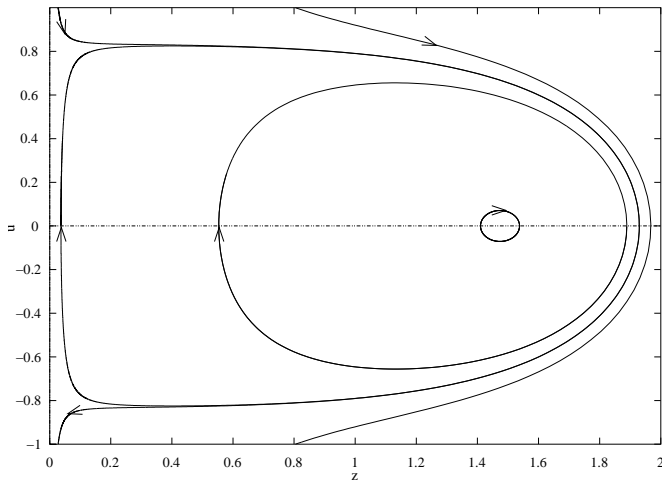


FIG. 2: The phase portrait of the system (25) in the projective coordinates  $(z, u)$  for the analysis of the behavior of trajectories at infinity. Two critical points appear at infinity  $(0, u_0 \pm)$ . They are of saddle type.

The two maps  $(z, u): z = 0, -\infty < u < \infty$  and  $(v, w): v = 0, -\infty < w < \infty$  cover the behavior of trajectories at the infinity circles  $x = \infty$  and  $y = \infty$ .

The original system

$$\begin{aligned}\dot{x} &= P(x, y), \\ \dot{y} &= Q(x, y),\end{aligned}$$

in the projective coordinates  $(z, u)$  and after the time reparameterization  $\tau \rightarrow \tau_1: d\tau_1 = x d\tau$  takes the form

$$\begin{aligned}\dot{z} &= zP^*(z, u), \\ \dot{u} &= Q^*(z, u) - uP^*(z, u),\end{aligned}$$

where

$$\begin{aligned}P^*(z, u) &= z^2 P(1/z, u/z), \\ Q^*(z, u) &= z^2 Q(1/z, u/z),\end{aligned}$$

and the dot denotes differentiation with respect to time  $\tau_1$ .

The representation of the dynamics as a one-dimensional Hamiltonian flow allows to make the classification of possible evolution paths in the configuration space which is complementary to phase diagrams. It also makes it simpler to discuss the physical content of the model. Finally, the construction of the Hamiltonian may allow to study brane quantum cosmology in full analogy to what is usually done in general relativity.

From equation (25) we can observe that the trajectories are integrable in quadratures. Namely, from the Hamiltonian constraint  $\mathcal{H} = E = 0$  we obtain the integral

$$t - t_0 = \int_{a_0}^a \frac{da}{\sqrt{-2V(a)}}. \quad (30)$$

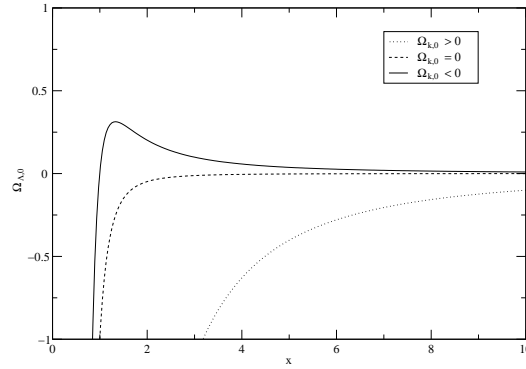


FIG. 3: The dependence of  $\Omega_{\Lambda_4}$  on  $x$ . The evolutionary path are represented by levels of constant  $\Lambda_4$ . Let us note that the domain under the characteristic curve  $\Omega_{\Lambda_4}(x)$  is non-physical.

Obviously, for a specific form of the potential function (26) we can obtain exact solutions. Some special cases have been already given in Section III.

It is possible to make a classification of the evolution paths by analyzing the characteristic curves which represent the boundary equation of the domain admissible for motion. For this purpose we consider the equation of zero velocity,  $\dot{a} = 0$  which constitutes the boundary  $\mathcal{M} = \{a: V(a) = 0\}$ .

From equations (21) and (22) the cosmological constant can be expressed as a function of  $x$  as follows

$$\Omega_{\Lambda_4,0}(x) = -x^{-2} (\Omega_{m,0} x^{-1} + \Omega_{\lambda,0} x^{-4} + \Omega_{k,0}), \quad (31)$$

where we have abbreviated  $\Omega_{GR}$  by  $\Omega_m$ . The plot of  $\Omega_{\Lambda_4,0}(x)$  for different  $k$  is shown in Fig. 3. Finally, we can consider the evolution path as a level of  $\Omega_{\Lambda_4,0} = \text{const}$  and then we can classify all the models with respect to their quantitative properties of the dynamics.

The present experimental estimates based on baryons in clusters, give  $\Omega_{m,0} \sim 0.3$ , and the location of the first peak in the CMB detected by Boomerang and Maxima suggests a flat universe. This implies that our Universe with the cosmological term is presently accelerating if (under the assumption of the dust  $\gamma = 1$  matter on the brane)

$$\Omega_{\Lambda_4,0} > \frac{1}{3} + \Omega_{\lambda,0}.$$

The required value of  $\Omega_{\lambda,0}$  seems to be unrealistic (see next section) and therefore the cosmological constant is still needed to explain the present acceleration of the Universe if we do not accept phantom type of matter.

#### IV. A REDSHIFT-MAGNITUDE RELATION FOR BRANE UNIVERSES

Cosmic distance indicators like the luminosity distance, depend sensitively on the spatial geometry (curvature) and on the present density parameters of different matter components and their form of the equation of state. For this reason a redshift-magnitude relation for distant galaxies is proposed as a potential test for the Friedmann brane model.

Let us consider an observer located at  $r = 0$  at the moment  $t = t_0$  which receives a light ray emitted at  $t = t_1$  from the source of the absolute luminosity  $L$  located at the radial distance  $r_1$ . The redshift  $z$  of the source is related to the scale factor  $a(t)$  at the two moments of evolution by  $1 + z = a(t_0)/a(t_1) \equiv a_0/a_1$ . If the apparent luminosity of the source as measured by the observer is  $l$ , then the luminosity distance  $d_L$  of the source is defined by the relation

$$l = \frac{L}{4\pi d_L^2} = \frac{L}{4\pi} \frac{1}{(1+z)^2 a_0^2 r_1^2}. \quad (32)$$

The observed and absolute luminosities are defined in terms of K-corrected apparent and absolute magnitudes  $m$  and  $\mathcal{M}$ . When written in terms of  $m$  and  $\mathcal{M}$ , Eq.(32) yields

$$m(z) = \mathcal{M} + 5 \log_{10}[\mathcal{D}_L(z)], \quad (33)$$

where  $\mathcal{M} = M - 5 \log_{10} H_0 + 25$ , and  $\mathcal{D}_L \equiv H_0 d_L$  is the dimensionless luminosity distance. For homogeneous and isotropic Friedmann models one gets [26]

$$\mathcal{D}_L(z) = \frac{(1+z)}{\sqrt{\mathcal{K}}} S(\chi) \quad (34)$$

where  $S(\chi) = \sin \chi$  for  $\mathcal{K} = -\Omega_{k,0}$ ;  $S(\chi) = \chi$  for  $\mathcal{K} = 0$ ;  $S(\chi) = \sinh \chi$  for  $\mathcal{K} = \Omega_{k,0}$ . From the Friedmann equation (12) and the form of the FRW metric we have

$$\chi(z) = \frac{1}{a_0 H_0} \int_0^z [f(z')]^{-1/2} dz', \quad (35)$$

where

$$f(z) \equiv \left\{ \Omega_{\lambda,0} (1+z')^{6\gamma} + \Omega_{GR,0} (1+z')^{3\gamma} + \Omega_{k,0} (1+z')^2 + \Omega_{\mathcal{U},0} (1+z')^4 + \Omega_{\Lambda_4,0} \right\}. \quad (36)$$

In order to understand the variability of  $\varrho^2$  contribution onto the dynamics of the brane universes which is formally described by the term  $\Omega_{\lambda,0}$  let us give a couple of particular examples. For instance, taking only the non-relativistic matter on the brane ( $\gamma_m = 1$ ) we can see that the luminosity distance can be written down as

$$d_L(z) = \frac{1+z}{H_0} \times \int_0^z \frac{dz'}{\sqrt{\Omega_{m,0}(1+z')^3 + \Omega_{\lambda m,0}(1+z')^6 + \Omega_{\Lambda_4,0}}}, \quad (37)$$

and the ‘brany’ dust contribution  $\Omega_{\lambda m,0}$  appears in front of  $(1+z')^6$ . If there is only radiation ( $\gamma_r = 4/3$ ) on the brane the luminosity distance reads as

$$d_L(z) = \frac{1+z}{H_0} \times \int_0^z \frac{dz'}{\sqrt{\Omega_{r,0}(1+z')^4 + \Omega_{\lambda r,0}(1+z')^8 + \Omega_{\Lambda_4,0}}}, \quad (38)$$

and the ‘brany’ radiation contribution  $\Omega_{\lambda r,0}$  appears in front of  $(1+z')^8$ . Another important example is the phantom matter on the brane ( $\gamma = -1/3$ ) which gives the luminosity distance in the form

$$d_L(z) = \frac{1+z}{H_0} \int_0^z \frac{dz'}{\sqrt{\frac{\Omega_{ph,0}}{(1+z')^2} + \frac{\Omega_{\lambda ph,0}}{(1+z')^2} + \Omega_{\Lambda_4,0}}}, \quad (39)$$

and the ‘brany’ phantom contribution  $\Omega_{\lambda ph,0}$  appears in front of  $(1+z')^{-2}$ .

In order to compare various matter on the brane models with the supernova data, we compute the distance modulus

$$\mu_0 = 5 \log(d_L) + 25$$

where  $d_L$  is in Megaparsecs. The goodness of a fit is characterized by the parameter

$$\chi^2 = \sum_i \frac{(\mu_{0,i}^0 - \mu_{0,i}^t)^2}{\sigma_{\mu_0,i}^2 + \sigma_{\mu z,i}^2}. \quad (40)$$

In (40)  $\mu_{0,i}^0$  is the measured value,  $\mu_{0,i}^t$  is the value calculated in the model described above,  $\sigma_{\mu_0,i}^2$  is the measurement error,  $\sigma_{\mu z,i}^2$  is the dispersion in the distance modulus due to peculiar velocities of galaxies.

We assume that supernovae measurements come with uncorrelated Gaussian errors and in this case the likelihood function  $\mathcal{L}$  can be determined from a  $\chi^2$  statistic  $\mathcal{L} \propto \exp(-\chi^2/2)$  [16, 19].

#### V. BRANE UNIVERSES TESTED BY SUPERNOVAE

We first test brane models using the sample A of Perlmutter SN Ia data. In order to avoid any possible selection effects we work with the full sample without excluding any supernova from that sample. It means that our basic sample is Perlmutter sample A. We checked our analysis using Perlmutter’s samples B and C but not significance difference was obtained. We estimate the model parameters using the best fit procedure. In the statistical analysis we also use the maximum likelihood method [16].

Firstly, we will study the case  $\gamma = 1$  (dust on the brane; we will label  $\Omega_{GR}$  by  $\Omega_m$ ). The case  $\gamma = 2/3$  (cosmic strings on the brane) has recently been studied in [28] where, in fact,  $\Omega_{\mathcal{U}}$  and  $\Omega_{\lambda}$  were neglected and

TABLE I: Results of the statistical analysis for the dust matter ( $\gamma = 1$ ) on the brane for the considered samples of SNIa. First two lines for each sample are the best fit model and the best fit flat model for the sample. Third line is the best fit flat model obtained by minimization over  $\mathcal{M}$ , while the last line is the best fit flat model with  $\Omega_{m,0} = 0.3$  obtained by minimization over  $\mathcal{M}$ .

| Sample | N   | $\Omega_{k,0}$ | $\Omega_{\lambda,0}$ | $\Omega_{m,0}$ | $\Omega_{\Lambda,0}$ | $\chi^2$ | $\mathcal{M}$ |
|--------|-----|----------------|----------------------|----------------|----------------------|----------|---------------|
| A      | 60  | -0.9           | 0.04                 | 0.59           | 1.27                 | 94.7     | -3.39         |
|        |     | 0.0            | 0.091                | 0.00           | 0.90                 | 94.7     | -3.39         |
|        |     | 0.0            | 0.087                | 0.00           | 0.91                 | 94.7     | -3.40         |
|        |     | 0.0            | 0.014                | 0.30           | 0.69                 | 95.7     | -3.37         |
| C      | 54  | -0.09          | 0.092                | 0.00           | 1.00                 | 52.5     | -3.44         |
|        |     | 0.0            | 0.080                | 0.00           | 0.92                 | 52.6     | -3.44         |
|        |     | 0.0            | 0.076                | 0.00           | 0.92                 | 52.6     | -3.40         |
|        |     | 0.0            | 0.004                | 0.30           | 0.70                 | 53.3     | -3.37         |
| K6     | 58  | -1.26          | -0.020               | 0.92           | 1.36                 | 55.0     | -3.52         |
|        |     | 0.0            | 0.076                | 0.00           | 0.92                 | 55.2     | -3.52         |
|        |     | 0.0            | 0.072                | 0.00           | 0.93                 | 55.2     | -3.53         |
|        |     | 0.0            | -0.004               | 0.30           | 0.70                 | 55.8     | -3.51         |
| K3     | 54  | -0.74          | -0.015               | 0.62           | 1.14                 | 60.3     | -3.48         |
|        |     | 0.0            | 0.056                | 0.02           | 0.92                 | 60.4     | -3.48         |
|        |     | 0.0            | 0.059                | 0.10           | 0.93                 | 60.4     | -3.48         |
|        |     | 0.0            | -0.011               | 0.30           | 0.71                 | 61.0     | -3.46         |
| TB1    | 218 | -0.02          | 0.087                | 0.00           | 0.93                 | 203.9    | 15.925        |
|        |     | 0.0            | 0.085                | 0.00           | 0.92                 | 203.9    | 15.925        |
|        |     | 0.0            | 0.078                | 0.00           | 0.92                 | 203.5    | 15.905        |
|        |     | 0.0            | 0.011                | 0.30           | 0.69                 | 208.3    | 15.925        |
| TB2    | 120 | 0.82           | -0.010               | 0.00           | 0.19                 | 89.5     | 15.925        |
|        |     | 0.0            | -0.020               | 0.54           | 0.48                 | 89.6     | 15.925        |
|        |     | 0.0            | -0.013               | 0.33           | 0.68                 | 90.3     | 15.905        |
|        |     | 0.0            | -0.002               | 0.30           | 0.70                 | 90.3     | 15.905        |
| TB3    | 98  | -0.18          | 0.104                | 0.00           | 1.08                 | 112.1    | 15.925        |
|        |     | 0.0            | 0.084                | 0.00           | 0.92                 | 112.5    | 15.925        |
|        |     | 0.0            | 0.088                | 0.13           | 0.78                 | 111.8    | 16.035        |
|        |     | 0.0            | 0.044                | 0.30           | 0.66                 | 112.4    | 16.035        |

where the term  $\Omega_{m,0}(1+z')^3$  was introduced in order to admit dust matter on the brane. This case was already presented in a different framework in Ref. [26]. Secondly, we will study the case  $\gamma = -1/3$  (phantom on the brane [20]) - we will label this type of matter with  $\Omega_{ph}$  instead of  $\Omega_{GR}$ .

Let us first estimate the value of  $\mathcal{M}$  from the full sample of 60 supernovae. For the flat  $\Lambda$ CDM model we obtained  $\mathcal{M} = -3.39$ . We use Perlmutter data and method of maximum likelihood estimation on this data to esti-

mate the different cosmological parameters of interest, i.e. pairs  $(\Omega_{m,0}, \Omega_{\lambda,0})$ ,  $(\Omega_{m,0}, \Omega_{\Lambda,0})$ .

The result of statistical analysis is presented in some figures and in Table I. Fig. 4 illustrates the confidence level as a function of  $(\Omega_{m,0}, \Omega_{\lambda,0})$  for the flat model ( $\Omega_{k,0} = 0$ ) minimized over  $\mathcal{M}$  with  $\Omega_{\Lambda,0} = 1 - \Omega_{m,0} - \Omega_{k,0} - \Omega_{\lambda,0}$ . In present cases we formally assume that both positive and negative values of  $\Omega_{\lambda,0}$  are mathematically possible although the negative values are in fact only possible if we admit the timelike extra dimensions [33]. We show that the preferred intervals for  $\Omega_{m,0}$  and  $\Omega_{\lambda,0}$  are  $\Omega_{m,0} < 0.4$  and  $\Omega_{\lambda,0} > 0$ .

We repeat our analysis for the case of  $\Omega_{k,0} \neq 0$ . The results of the statistical analysis are presented in Table I. Two upper lines for each sample are best fit model and best fit flat model for sample with fixed  $\mathcal{M}$  as obtained for the flat  $\Lambda$ CDM. Third line is best fit flat model obtain with minimization over  $\mathcal{M}$  while last line is best fit flat model with  $\Omega_{m,0} = 0.3$  (preferred by present extragalactic data [34]) obtained with minimization over  $\mathcal{M}$ .

One should note that the result obtained for Perlmutter's sample C is a little bit different than the one obtained in preliminary analysis [32] for  $\mathcal{M} = -3.39$  ( $\Omega_{k,0} = 0$ ,  $\Omega_{m,0} = 0.21$ ,  $\Omega_{\lambda,0} = 0.048$   $\Omega_{\Lambda,0} = 0.75$ ). It reflects the sensitivity of the results to changes of  $\mathcal{M}$  parameter.

The Perlmutter data were gathered four years ago, hence it would be interesting to use more recent supernovae data as well. We decided to test our model using this new sample of supernovae. Recently Knop et al. [35] have reexamined the Perlmutter's data with host-galaxy extinction correctly assessed. The mentioned authors distinguished few subsets of supernovae from this sample. We consider two of them. The first is a subset of 58 supernovae with extinction correction (Knop subsample 6; hereafter K6) and the second one a sample of 54 supernovae with low extinction (Knop subsample 3; hereafter K3). Sample C and K3 are similarly constructed because both contain only low extinction supernovae.

Another sample was presented by Tonry *et al.* [36] who collected a large number of supernovae published by different authors and added eight new high redshift SN Ia. This sample of 230 SNe Ia was recalibrated with consistent zero point. Whenever it was possible, the extinctions estimates and distance fitting were recomputed. However, none of the methods was able to be applied to all supernovae (for details see Table 8 in [36]). This sample was improved by Barris who added 23 high redshift supernovae including 15 at  $z \geq 0.7$  doubling the published number of object at this redshifts [37].

Despite of these problems, the analysis of our model using this sample seems to be interesting. We decided to analyze the sample of 218 SNe Ia (hereafter sample TB1) which consists of low extinction supernovae only (median V band extinction  $A_V < 0.5$ ).

Tonry and Barris [36, 37] presented redshift and luminosity distance observations for their sample of supernovae. Therefore, Eqs. (23a) and (23b) should be modi-

fied [38]:

$$m - M = 5 \log_{10}(\mathcal{D}_L)_{\text{Tonry}} - 5 \log_{10} 65 + 25 \quad (41)$$

and

$$\mathcal{M} = -5 \log_{10} H_0 + 25. \quad (42)$$

For  $H_0 = 65 \text{ km s}^{-1} \text{ Mpc}^{-1}$ , we obtain  $\mathcal{M} = 15.935$ .

The results obtained for the flat model with the Tonry/Barris sample of 218 SNIa is very similar to that obtained for flat model with the Perlmutter sample. However, even then we allowed  $\Omega_{k,0} \neq 0$  than for TBI sample we obtained that preferred model of the universe is nearly flat one, which is in agreement with CMBR data. It is the advantage of our model in comparison to  $\Lambda$ CDM model, where [16, 19] the high negative value of  $\Omega_{k,0}$  was the best fit, although  $\Omega_{k,0}$  is also statistically admissible. In order to find the curvature, they additionally used the data from CMBR and extragalactic astronomy.

We also confront our model against Knop's sample. While for the flat model we obtained similar results than for the previous samples, in the case without of any priors on  $\Omega_{k,0}$  Knop's sample prefers its highly negative values together with the negative values of  $\Omega_{\lambda,0}$ . Note, however that it is an unphysical case, because the brane tension should be positive unless timelike extra dimensions are admitted [33]. One should note that with this assumption the Knop's sample suggests ( $\Omega_{m,0} < 0.3$  which is in agreement with the result obtained for this sample in the case of  $\Lambda$ CDM model [35]).

Applying the marginalization procedure over  $\Omega_{k,0}$ ,  $\Omega_{\lambda,0}$ ,  $\mathcal{M}$  for the Perlmutter sample A we find the lowest value of  $\chi^2$  for each pair of values ( $\Omega_{m,0}, \Omega_{\Lambda,0}$ ) as shown in Fig. 5. The favoured intervals for ( $\Omega_{m,0}, \Omega_{\Lambda,0}$ ) are  $\Omega_{m,0} < 0.5$  and  $\Omega_{\Lambda,0} \simeq 1.3$ . As the best fit we obtain:  $\Omega_{k,0} = -0.48$ ,  $\Omega_{m,0} = 0$ ,  $\Omega_{\lambda,0} = 0.14$ , and  $\mathcal{M} = -3.43$ . There is a marginal difference between that result and the one obtained for  $\mathcal{M} = -3.39$ . Another example is that for  $\mathcal{M} = -3.39$  and  $\Omega_{k,0} = -0.20$ , ( $\Omega_{m,0} = 0$ ,  $\Omega_{\lambda,0} = 0.118$ ,  $\Omega_{\Lambda,0} = 1.08$  and for the case noted in the first line of tab I we obtain nearly the same  $\chi^2$  value.

In fact, we obtained a 3D ellipsoid in a 3d parameter space  $\Omega_{m,0}, \Omega_{\lambda,0}, \Omega_{\Lambda,0}$ . Then, we have more freedom than in the case of analysis of Ref. [19], where there was only an ellipse in a 2D parameter space  $\Omega_{m,0}$  and  $\Omega_{\Lambda,0}$ . It clearly demonstrates that the results obtained from the best-fit analysis should be supported by the analysis of the confidence levels for the parameter intervals obtained from maximum likelihood method. Support from CMBR and extragalactic astronomy results may also be useful.

In the case of  $\Omega_{k,0} \neq 0$ , the confidence level for values of pairs ( $\Omega_{m,0}, \Omega_{\Lambda,0}$ ) (Perlmutter sample A) are shown in the standard way after minimizing over  $\mathcal{M}$ ,  $\Omega_{k,0}$ ,  $\Omega_{\lambda,0}$  in Fig. 6. One can see that a non-zero cosmological constant is required in our model. This analysis was repeated with fixed value of  $\mathcal{M} = -3.39$  (Fig. 7). These figures shows that procedure of the minimizing over  $\mathcal{M}$ , however important, is not crucial for selecting preferred intervals of ( $\Omega_{m,0}, \Omega_{\Lambda,0}$ ) in our model.

In Fig. 8 we presented confidence levels in the plane ( $\Omega_{m,0}, \Omega_{\Lambda,0}$ ) for TBI sample. The allowed area is in agreement with that obtained for the Perlmutter sample, but significantly smaller. The earlier conclusion that the non-zero cosmological constant is required is confirmed. However, as we will see further, the admission of strongly negative pressure matter (phantom) on the brane does not require cosmological constant.

Padmanabhan and Choudhury [39, 40] suggest that dividing the sample into the low and high redshift supernovae gives interesting results. They obtained that although the full data sets of SNIa strongly rules out models without dark energy, the high and low redshift data sets individually, admit decelerating models with zero dark energy [39, 40]. We decide to check this result in the case of our model. We divide TBI sample for 120 low redshift SNIa with  $z \leq 0.25$  (TB2 sample) and 98 high redshift SNIa with  $z > 0.25$  (sample TB3). The results are presented in Table I and in Figs. 9 - Fig. 10. One can see that the preferred values of the model parameters are different in both cases. For low redshifts  $z \leq 0.25$  the data sets taken individually results in decelerating models without cosmological constant, while for high redshift  $z > 0.25$  data sets it requires the non-zero cosmological constant. It confirms that pure low redshift data cannot be used for discrimination between cosmological models effectively (see [39]).

One should note, that the present extragalactic data for galaxy clusters (cluster baryon fraction) with CMB anisotropy measurement prefer a flat model ( $\Omega_{k,0}$ ) with  $\Omega_{m,0} \simeq 0.3$  [34]. For a deeper statistical analysis of brane expansion scenario in explaining the currently accelerating universe we consider 1D plot of the density distribution of  $\Omega_{\lambda,0}$ . From this analysis one can obtain the limits at the  $1\sigma$  level. Fig. 11 shows the density distribution for  $\Omega_{\lambda,0}$  in the flat model with  $\Omega_{m,0} = 0.3$ . This distribution is obtained from the marginalization over  $\mathcal{M}$ . On the base of the noted above results we assumed that "true" value of  $\mathcal{M}$  is in the interval  $[-3.37, -3.44]$  and that interval we take into account during the marginalization procedure. One can conclude that with the probability of 68.3 we get  $\Omega_{\lambda,0} < 0.019$  while with the probability 95.4 we get  $\Omega_{\lambda,0} < 0.037$ .

If we formally consider the possibility of a negative value of  $\Omega_{\lambda,0}$  which can be interpreted as the negative brane tension with dust on the brane [23] the corresponding distribution function is shown in Fig. 12. One can see that  $\Omega_{\lambda,0} < 0.020$  on the  $1\sigma$  confidence level and  $\Omega_{\lambda,0} < 0.038$  on the  $2\sigma$  confidence level with preferred value  $\Omega_{\lambda,0} = 0.004$ . However, the error in estimation is so large that possibility that  $\Omega_{\lambda,0} = 0$  cannot be excluded. One should note, that when we formally increase the analyzed interval of  $\mathcal{M}$  to  $[-3.29, -3.49]$  we obtain the preferred value  $\Omega_{\lambda,0} = 0.013$ . Also, the errors in estimation increase and  $\Omega_{\lambda,0} < 0.037$  on the  $1\sigma$  confidence level and  $\Omega_{\lambda,0} < 0.061$  on the  $2\sigma$  confidence level. It demonstrates the sensitivity of the results of estimation of  $\Omega_{\lambda,0}$  with respect to small changes of  $\mathcal{M}$  parameter.



In the near future the SNAP mission is expected to observe about 2000 type Ia supernovae each year, over a period of three years [52]. Therefore it could be possible to verify hypothesis that  $\Omega_{\lambda,0} > 0$  because errors in the estimation of  $\Omega_{\lambda,0}$  will decrease significantly. We test how large number of new data should influence on errors in estimation of  $\Omega_{\lambda,0}$ . We assume that the Universe is flat with  $\Omega_{m,0} = 0.28$ ,  $\Omega_{\lambda,0} = 0.01$  and  $\mathcal{M} = -3.39$ . For the model with dust matter on the brane we generate the sample of 1000 supernovae randomly distributed in the redshift range  $0.01 < z < 2$ . We assume a Gaussian distribution of uncertainties in the measured values of  $m$  and  $z$ . The errors in redshifts  $z$  are of order  $1\sigma = 0.002$  while the uncertainty in a measurement of the magnitude  $m$  is assumed as  $1\sigma = 0.15$ . The systematic uncertainty limits is  $\sigma_{sys} = 0.02$  mag at  $z = 1.5$  [41] which means that  $\sigma_{sys}(z) = (0.02/1.5)z$ . For the sample generated in such a way we should now repeat our analysis. The error for  $\Omega_{\lambda,0} \simeq 0.0007$  on the confidence level of 68.3, while  $\Omega_{\lambda,0} \simeq 0.0013$  is on the confidence level 95.4. It is clearly confirmed that the error in measurement of  $\Omega_{\lambda,0}$  from supernovae data will decrease significantly in the new future.

In Fig. 14 we present the plot of residuals of redshift-magnitude relationship for the supernovae data for  $\Omega_{m,0} = 0.3$ . We present the residuals between the Einstein-de Sitter model and Perlmutter model, best fitted flat brane model and best fitted brane model. As a result, with the increasing impact of  $\Omega_{\lambda,0}$  (higher  $\Omega_{\lambda,0}$ ) the high-redshift supernovae should be brighter than the expected by the Perlmutter model. Let us note that for the best-fit value of  $\Omega_{\lambda,0} = 0.020$ , the difference between the brane model and the Perlmutter model should be detectable for  $z > 1.2$  (because  $\Delta m \geq 0.2$ ). One should observe that there is a small difference between the best fit flat model (with minimal value of  $\chi^2$ ) where we obtain  $\Omega_{\lambda,0} = 0.006$  and the value obtained from the minimization procedure  $\Omega_{\lambda,0} = 0.004$  (see Fig. 12).

For comparison we presented the best fits (Fig. 15) without a specifically assumed value of  $\Omega_{m,0}$ . This latter case is, characterized by greater expected differences between the brane model and the Perlmutter model for high redshift supernovae.

The above prediction for brane models that the high redshift supernovae are *brighter than expected* in  $\Lambda$ CDM (Perlmutter) model could also be detectable by the new SNAP data. It gives a possibility to discriminate between predictions of the two models. Of course similar effect is expected for galaxies, but for an extended object such an effect is much more difficult to detect than for the point sources.

In Fig. 16 we present the difference in redshift-magnitude relation (35) for brane models with phantom matter on the brane ( $\gamma = -1/3$ ) using Perlmutter's sample A. Note that the theoretical curves are very close to that of [19] which means that the phantom cancels the positive-pressure influence of the  $\varrho^2$  term and can *mimic* the negative-pressure influence of the cosmological

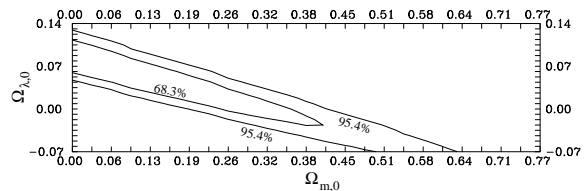


FIG. 4: Confidence levels in the plane  $(\Omega_{m,0}, \Omega_{\lambda,0})$  minimized over  $\mathcal{M}$  for the flat model, and with  $\Omega_{\Lambda_4,0} = 1 - \Omega_{m,0} - \Omega_{k,0} - \Omega_{\lambda,0}$ . The figure shows the ellipses of the preferred values of  $\Omega_{m,0}$  and  $\Omega_{\Lambda_4,0}$ . The results prefer positive values of  $\Omega_{\lambda,0}$ , but negative values are allowed as well (Perlmutter sample A).

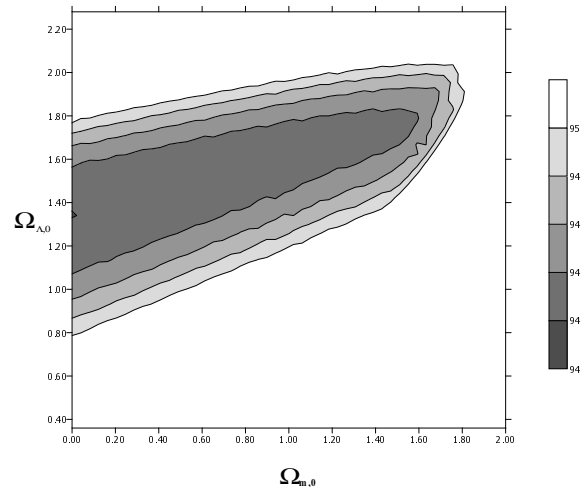


FIG. 5: The levels of constant  $\chi^2$  in the plane  $(\Omega_{m,0}, \Omega_{\Lambda_4,0})$  marginalized over  $\mathcal{M}$ , and with  $\Omega_{\Lambda_4,0} = 1 - \Omega_{m,0} - \Omega_{k,0} - \Omega_{\lambda,0}$ . The figure shows the preferred values of  $\Omega_{m,0}$  and  $\Omega_{\Lambda_4,0}$  (Perlmutter sample A).

constant to cause cosmic acceleration. From the formal point of view the best fit is ( $\chi^2 = 95.4$ ) for  $\Omega_{k,0} = 0.2$ ,  $\Omega_{ph,0} = 0.7$ ,  $\Omega_{\lambda,0} = -0.1$ ,  $\Omega_{\mathcal{U}} = 0.2$ ,  $\Omega_{\Lambda_4,0} = 0$  which means that the cosmological constant must necessarily *vanish*. From this result we can conclude that phantom matter  $p = -(4/3)\varrho$  can *mimic* the contribution from the  $\Lambda_4$ -term in standard models. For the best-fit flat model ( $\Omega_{k,0} = 0$ ) we have ( $\chi^2 = 95.4$ ):  $\Omega_{ph,0} = 0.2$ ,  $\Omega_{\lambda,0} = -0.1$ ,  $\Omega_{\mathcal{U}} = 0.2$ ,  $\Omega_{\Lambda_4,0} = 0.7$ .

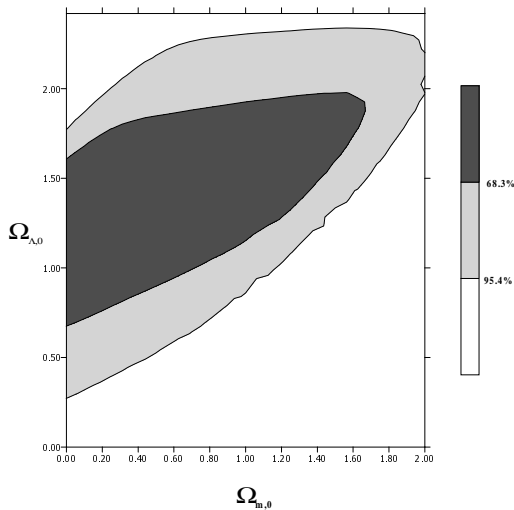


FIG. 6: Confidence levels in the plane  $(\Omega_{m,0}, \Omega_{\Lambda_4,0})$  minimized over  $\mathcal{M}$ , and with  $\Omega_{\Lambda_4,0} = 1 - \Omega_{m,0} - \Omega_{k,0} - \Omega_{\lambda,0}$ . The figure shows the ellipses of the preferred values of  $\Omega_{m,0}$  and  $\Omega_{\Lambda_4,0}$  (Perlmutter sample A).

## VI. ANGULAR DIAMETER SIZE AND THE AGE OF THE UNIVERSE

Another cosmological test which can be performed is the angular diameter size

$$\theta = \frac{d(z+1)^2}{d_L} \quad (43)$$

of a galaxy with a linear size  $d$ . In a flat dust ( $\gamma = 1$ ) universe  $\theta$  has the minimum value  $z_{min} = 5/4$ . It is particularly interesting to notice that for flat brane models with  $\Omega_{\lambda} \approx 0, \Omega_{\Lambda_4} \approx 0$  the dark radiation can *enlarge* the minimum value of  $\theta$  while the ordinary radiation lowers this value [25], i.e.,

$$z_{min} = \frac{1}{2\mathcal{U}} \left( \Omega_{\mathcal{U}} - 1 + \sqrt{3\Omega_{\mathcal{U}} + 1} \right) \geq \frac{5}{4} \quad (44)$$

for  $\Omega_{\mathcal{U}} \leq 0$ . This is a general influence of negative dark radiation onto the angular diameter size for brane models. One can also notice that there exists a restriction on the amount of negative dark radiation coming from (44) ( $\Omega_{\mathcal{U}} \geq -1/3$ ) which can serve as a test for the admissible value of  $\Omega_{\mathcal{U}} = -1/3$  ( $z_{min} = 2$ ) in order to observe the minimum.

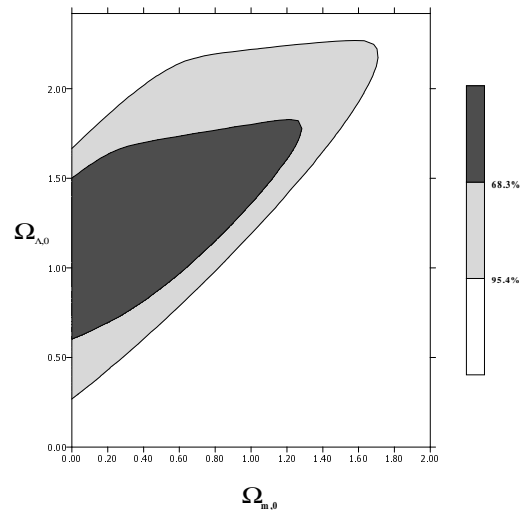


FIG. 7: Confidence levels in the plane  $(\Omega_{m,0}, \Omega_{\Lambda_4,0})$ ,  $\mathcal{M} = -3.39$ , and with  $\Omega_{\Lambda_4,0} = 1 - \Omega_{m,0} - \Omega_{k,0} - \Omega_{\lambda,0}$ . The figure shows the ellipses of the preferred values of  $\Omega_{m,0}$  and  $\Omega_{\Lambda_4,0}$  (Perlmutter sample A).

More detailed analytic and numerical studies show that the increase of  $z_{min}$  is even more sensitive to negative values of  $\Omega_{\lambda}$  which, unfortunately, are admissible only for timelike extra dimensions [33]. Similarly as for the dark radiation  $\Omega_{\mathcal{U}}$ , the minimum disappears for some large negative  $\Omega_{\lambda}$ . Positive  $\Omega_{\mathcal{U}}$  and  $\Omega_{\lambda}$  make  $z_{min}$  decrease. In Fig. 17 we present a plot from which one can see the sensitivity of  $z_{min}$  to  $\Omega_{\mathcal{U}}$ .

As far as a possible contribution of  $\Omega_{\lambda}$  is concerned, then from Fig. 18 we can see that its influence on the angular size  $\theta$  is relatively weak. As a conclusion we can say that it is possible to test values of  $\Omega_{\mathcal{U},0}$  and  $\Omega_{\lambda,0}$  from the angular diameter minimum value test, but because of the evolutionary effects and observational difficulties the predicted differences are too small to be detect. We have also checked that phantom matter  $\Omega_p h$  has very little influence onto the value of  $z_{min}$ .

Now let us briefly discuss the effect of brane parameters and phantom matter onto the age of the universe which according to (12) is given by

$$H_0 t_0 = \int_0^1 \left\{ \Omega_{GR,0} x^{-3\gamma+4} + \Omega_{\lambda,0} x^{-6\gamma+4} + \Omega_{\mathcal{U},0} + \Omega_{k,0} x^2 + \Omega_{\Lambda_4,0} x^4 \right\}^{-\frac{1}{2}} x dx, \quad (45)$$

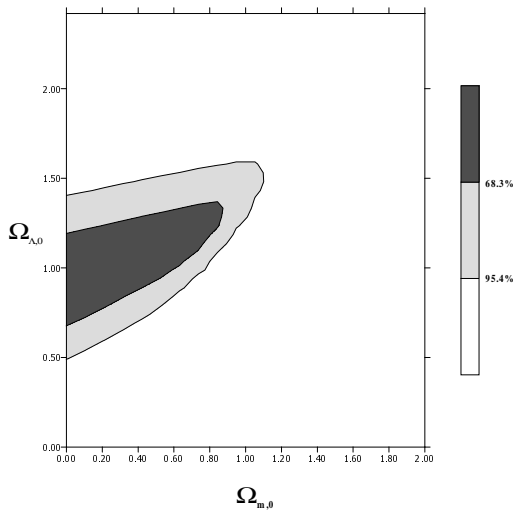


FIG. 8: Confidence levels in the plane  $(\Omega_{m,0}, \Omega_{\Lambda_4,0})$  for the sample Tonry/Barris 218 low extinguished SNIA.

where  $x = a/a_0$ . We made a plot for the dust  $\gamma = 1$  on the brane in Fig.19 which shows that the effect of quadratic in energy density term represented by  $\Omega_\lambda$  is to *lower* significantly the age of the universe.

For the dust matter and the cosmological constant the age of universe is given by

$$t_0 = \frac{1}{3H_0\sqrt{\Omega_{\Lambda,0}}} \ln \frac{\Omega_{m,0} + 2\Omega_{\Lambda,0} + 2\sqrt{\Omega_{\Lambda,0}}}{\Omega_{m,0} + \sqrt{4\Omega_{\Lambda,0}\Omega_{\Lambda,0}}}. \quad (46)$$

In Fig. 21 we made another plot of (46) in Gyrs for the flat model for different  $\Omega_{\lambda,0}$ . We can again see that the dust matter on the brane which mimics brane contribution as stiff-fluid decreases significantly the age of the universe.

The problem can be avoided, if we *accept* phantom  $\gamma = -1/3$  on the brane [20], since the phantom has a very strong influence to increase the age. In Fig. 20 we made a plot for this case which shows how phantom energy enlarges the age.

Therefore the *cosmological constant* or the *phantom matter* is needed to explain the problem of the age of the universe.

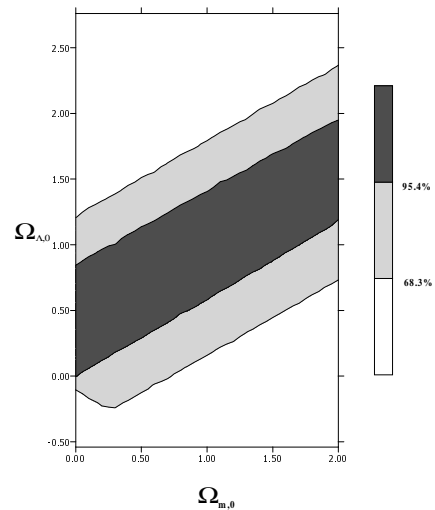


FIG. 9: Confidence levels in the plane  $(\Omega_{m,0}, \Omega_{\Lambda_4,0})$  for the sample Tonry/Barris 120 low extinguished SNIA with  $z \leq 0.25$ . The figure illustrate that with sample of low redshift supernovae we obtain that model without cosmological constant is statistically admissible.

## VII. DOPPLER PEAKS

The CMB peaks arise from acoustic oscillations of the primeval plasma. Physically, these oscillations are represented by hot and cold spots in CMB temperature. A wave which had a maximum of the density at the time of the last scattering corresponds to a peak in the power spectrum. In the Legendre multipole space this corresponds to an appropriate angle  $\theta_a$  subtended by the sound horizon at the last scattering surface. Higher harmonics of the principal oscillations, which have oscillated more than once, correspond to secondary peaks.

For our purpose it is very important that the location of these peaks are very sensitive to the variations in the model parameters. Therefore, it can be used as a probe to constrain the cosmological parameters and discriminate among various models.

If  $\theta_a$  is the angular size of the density fluctuation, then the acoustic scale for the peaks is  $(l_a = \pi/\theta_a)$  [31]

$$l_a = \pi \frac{\int_0^{z_{dec}} [f(z')]^{-1/2} dz'}{\int_{z_{dec}}^{\infty} c_s [f(z')]^{-1/2} dz'} \quad (47)$$

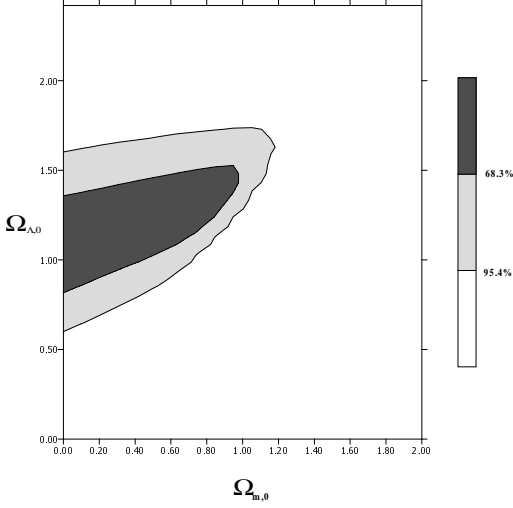


FIG. 10: Confidence levels in the plane  $(\Omega_{m,0}, \Omega_{\Lambda,0})$  for the sample Tonry/Barris of 98 low extinguished SNIa with  $z > 0.25$ .

( $z_{dec} = 1100$ ) where  $c_s$  is the speed of sound and the position of the peaks is

$$l_i = l_a(i - \phi_i) \quad (48)$$

( $i = 1, 2, 3$ ), where the phase shift [42, 43]

$$\phi_i \approx 0.267 \left[ \frac{r(z_{dec})}{0.3} \right]^{0.1}. \quad (49)$$

The phase shift is caused by the pre-recombination physics (plasma driving effect) and, hence, has no significant contribution from the term containing brane in that epoch so that it was taken from standard cosmology. We take  $\Omega_{b,0}h^2 = 0.02$ ,  $r(z_{dec}) \equiv \rho_r(z_{dec})/\rho_m(z_{dec}) = \Omega_{r,0}(1+z_{dec})/\Omega_{m,0}$ ,  $\Omega_{r,0} = \Omega_{\gamma,0} + \Omega_{\nu,0}$ ,  $\Omega_{\gamma,0} = 2.48h^{-2} \cdot 10^{-5}$ ,  $\Omega_{\nu,0} = 1.7h^{-2} \cdot 10^{-5}$ ,  $r(z_{dec})$  is the ratio of radiation to matter densities at the surface of last scattering and we have  $\Omega_{r,0} = 9.89 \cdot 10^{-5}$ ,  $\Omega_{b,0} = 0.05$ , and the spectral index for initial density perturbations  $n = 1$ , and  $h = 0.65$  [44].

For dust matter  $\Omega_{m,0}$ , radiation  $\Omega_{r,0}$ , and dark radiation  $\Omega_{\mathcal{U},0}$  ( $\Omega_{\gamma,0} = \Omega_{r,0} + \Omega_{\mathcal{U},0}$ ) on the brane under the assumption that we neglect the influence of the quadratic in energy density term of radiation  $\Omega_{r,0}$  we have the effective speed of sound

$$c_{eff}^2 = c_s^2 + \frac{\Omega_{b,0}(1+z)^3 + \frac{4}{3}\Omega_{\gamma,0}(1+z)^4}{\Omega_{\tilde{\lambda},0} + \Omega_{b,0}(1+z)^3 + \Omega_{\gamma,0}(1+z)^4}, \quad (50)$$

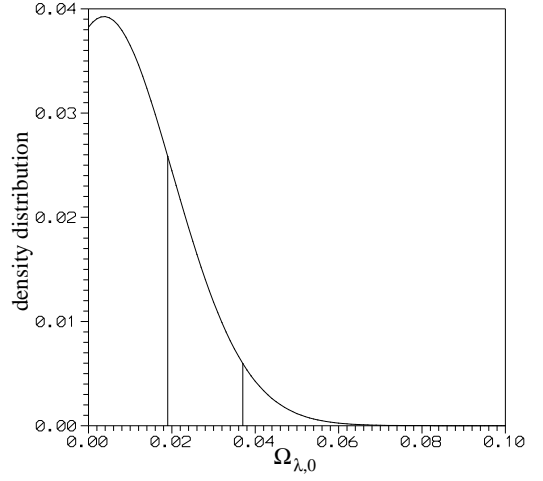


FIG. 11: The density distribution for  $\Omega_{\lambda,0}$  in the model with (only positive) brane fluid present. We obtain the limit  $\Omega_{\lambda,0} < 0.019$  at the confidence level 68.3, and  $\Omega_{\lambda,0} < 0.037$  at the confidence level 95.4 ( $\Omega_{m,0} = 0.3$ , Perlmutter sample A)

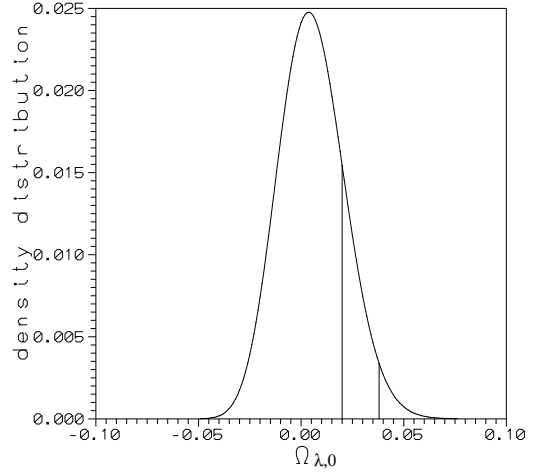


FIG. 12: The density distribution for  $\Omega_{\lambda,0}$  in the brane model. We obtain that  $\Omega_{\lambda,0} < 0.020$  at  $1\sigma$  level and  $\Omega_{\lambda,0} < 0.038$  at  $2\sigma$  level. Both positive and negative values of  $\Omega_{\lambda,0}$  are formally possible. For simplicity, we only mark limits on the positive side. ( $\Omega_{m,0} = 0.3$ , Perlmutter sample A).

with  $c_s^2$  of the same form as in standard cosmology and

$$\Omega_{\tilde{\lambda},0} = \frac{\Omega_{m,0}^2}{2\Omega_{\lambda,0}}. \quad (51)$$

The influence of brane on the location of the peaks is to shift them towards higher values of  $l$ . For example, for  $\Omega_{m,0} = 0.3$ ,  $\Omega_{b,0} = 0.05$ ,  $h = 0.65$ , the different choices of  $\Omega_{\lambda,0}$  yield the following

$$\begin{aligned} \Omega_{\lambda,0} = 0: & l_{\text{peak},1} = 225, l_{\text{peak},2} = 535, l_{\text{peak},3} = 847 \\ \Omega_{\lambda,0} = 1.5 \cdot 10^{-15}: & l_{\text{peak},1} = 227, l_{\text{peak},2} = 540, l_{\text{peak},3} = 853, \\ \Omega_{\lambda,0} = 10^{-12}: & l_{\text{peak},1} = 239, l_{\text{peak},2} = 568, l_{\text{peak},3} = 897. \end{aligned}$$

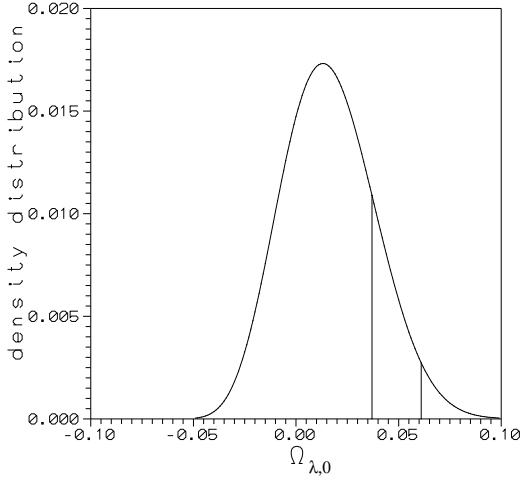


FIG. 13: The density distribution for  $\Omega_{\lambda,0}$  in the brane model (with  $\mathcal{M}$  in the interval  $[-3.29; 3.49]$ ). We obtain that  $\Omega_{\lambda,0} = 0.013$  and  $\Omega_{\lambda,0} < 0.037$  at  $1\sigma$  level and  $\Omega_{\lambda,0} < 0.061$  at  $2\sigma$  level. Both positive and negative values of  $\Omega_{\lambda,0}$  are formally possible. For simplicity, we only mark limits on the positive side. ( $\Omega_{m,0} = 0.3$ , Perlmutter sample A).

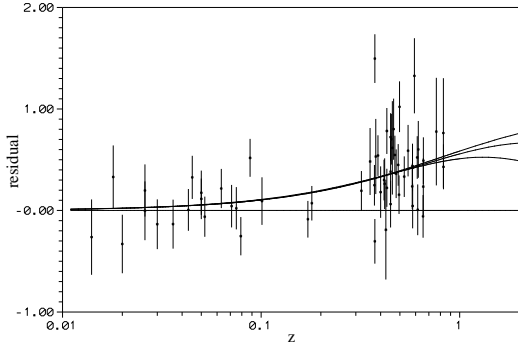


FIG. 14: Residuals (in mag) between the Einstein-de Sitter model and: the Einstein-de Sitter model itself (zero line), the Perlmutter flat model (upper curve), the  $\Omega_{m,0} = 0.3$  the best-fit flat brane model ( $\Omega_{\lambda,0} = 0.006$  and  $\Omega_{k,0} = 0$ ) (upper-middle curve), and  $\Omega_{m,0} = 0.3$  best-fit brane model ( $\Omega_{\lambda,0} = 0.020$ ,  $\Omega_{k,0} = -0.1$ ) (lower-middle curve).

We could also analyze the influence of dark radiation term in the brane world cosmology. The corresponding term in this case scales just like radiation with a constant  $\rho_0$  and both positive and negative values of  $\rho_{r,0}$  ( $\rho_{u,0}$ ) are possible. Dark radiation should strongly affect both the BBN and CMB. Ichiki *et al.* [45] used such observations to constrain both the magnitude and the sign of dark radiation in the case when the  $\rho^2$  term coming from the brane is negligible. We take their limits on dark radiation with negative contribution because of the tension between the observed  ${}^4\text{He}$  and  $D$  abundance [45]. In our case we take into consideration the brane term  $\rho^2$  and obtain the following positions of the first three peaks:

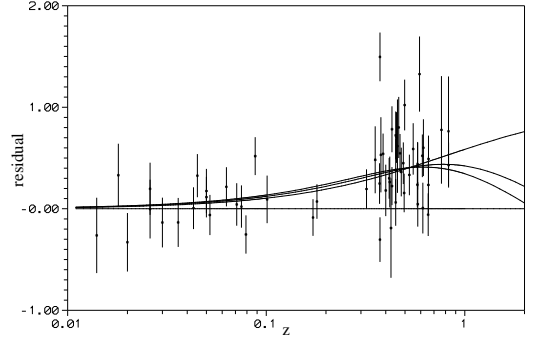


FIG. 15: Residuals (in mag) between the Einstein-de Sitter model and: the Einstein-de Sitter itself (zero line), the Perlmutter flat model (upper curve), the best-fit flat brane model (upper-middle curve),  $\Omega_{k,0} = 0$ ,  $\Omega_{m,0} = 0.25$ ,  $\Omega_{\lambda,0} = 0.02$ ,  $\Omega_{\Lambda_4,0} = 0.73$  and the best-fit brane (lower-middle curve)  $\Omega_{k,0} = -0.9$ ,  $\Omega_{m,0} = 0.59$ ,  $\Omega_{\lambda,0} = 0.04$ ,  $\Omega_{\Lambda_4,0} = 1.27$ .

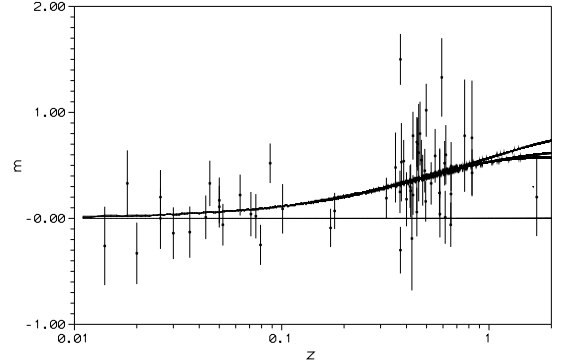


FIG. 16: Residuals (in mag) in redshift-magnitude relation for  $\gamma = -1/3$  brane universes (phantom matter on the brane). The top line is the best-fit flat model of Ref. [19] with  $\Omega_{m,0} = 0.28$ ,  $\Omega_{\Lambda_{(4)},0} = 0.72$ . The bottom line is a pure flat model with  $\Omega_{\Lambda_{(4)},0} = 0$ . Between - two brane models with  $\Omega_{\lambda,0} \neq 0$ : lower - the best-fit model; higher - the best-fit *flat* model. The brane phantom plots are very close to the top line of Ref. [19].

$$\begin{aligned} \Omega_{u,0} = -1.23\Omega_{\gamma,0} \quad \Omega_{\lambda,0} = 10^{-12}: \quad & l_{\text{peak},1} = 208, \quad l_{\text{peak},2} = 495, \\ & l_{\text{peak},3} = 781, \\ \Omega_{u,0} = -\Omega_{\gamma,0} \quad \Omega_{\lambda,0} = 10^{-12}: \quad & l_{\text{peak},1} = 214, \quad l_{\text{peak},2} = 545, \\ & l_{\text{peak},3} = 861, \\ \Omega_{u,0} = -0.41\Omega_{\gamma,0} \quad \Omega_{\lambda,0} = 10^{-12}: \quad & l_{\text{peak},1} = 229 \quad l_{\text{peak},2} = 545, \\ & l_{\text{peak},3} = 861. \end{aligned}$$

From Boomerang observations [46] we obtain  $l_{\text{peak},1} = 200 - 223$ ,  $l_{\text{peak},2} = 509 - 561$ . Therefore, uncertainties in values  $l_{\text{peak}}$  can be used in constraining cosmology with brane effect, namely

$$\Omega_{\lambda,0} \leq 1.0 \cdot 10^{-12}$$

from the location of the first peak.

We also compare the results from the above procedure with recent bounds on the location of the first two peaks obtained by WMAP collaboration [47, 48] namely  $l_{\text{peak},1} = 220.1 \pm 0.8$ ,  $l_{\text{peak},2} = 546 \pm 10$ , together with

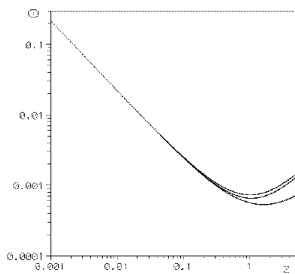


FIG. 17: The angular diameter  $\theta$  for  $\Omega_\lambda = 0.1, \Omega_m = 0.3, \Omega_{\Lambda_4} = 0.72$ , and the two values of  $\Omega_U = 0.1, -0.1$  (top, middle) in comparison with the model of Ref. [19] with  $\Omega_m = 0.28, \Omega_{\Lambda_4} = 0.72$  (bottom).

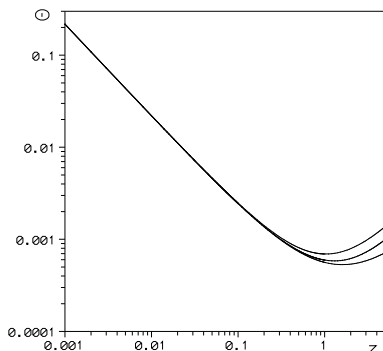


FIG. 18: The angular diameter  $\theta$  for the flat brane model for  $\Omega_{m,0} = 0.3$  and  $\Omega_{\lambda,0} = 0.1, 0.02, 0$  (top, middle, bottom, respectively). The minima for these cases are 1.04, 1.30, 1.605, respectively. The brane fluid causes the minimum to move left (towards to lower  $z$ ) and the minimum value of  $\theta$  increases.

the bound on the location of the third peak obtained by Boomerang collaborations  $l_{\text{peak},3} = 825^{+10}_{-13}$  which lead to quite strong constraints on the model parameters. These constraints can be summarized as follows. If we assume no dark radiation, the brane model is in agreement with observations provided we take

$$\Omega_{\lambda,0} \leq 1.0 \cdot 10^{-15}$$

We have made similar considerations for phantom on the brane (with matter and radiation included - otherwise the speed of sound becomes imaginary, compare Ref. [29]) and obtained the limit  $\Omega_{\lambda,0} \leq 1.0 \times 10^{-13}$  for  $\Omega_m = 0.3, \Omega_{ph,0} = 0.7 - \Omega_{\gamma,0}, \Omega_{k,0} = 0$  and the location of the peaks is at  $l_1 = 225, l_2 = 535, l_3 = 845$ .

However, the phase shift  $\phi$  in the above considerations is taken from the standard cosmology, i.e., we assume that the contribution from the brane term is insignificant at the pre-recombination epoch. If this assumption was not valid then the limit from CMB would change.

## VIII. BIG-BANG NUCLEOSYNTHESIS

It is clear from the Friedmann equation (10) that the brane models with positive pressure  $\gamma > 1$  matter lead to

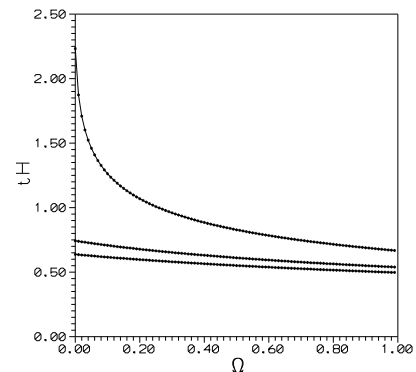


FIG. 19: The age of the universe  $t_0$  in units of  $H_0^{-1}$  for the brane models with dust ( $0 \leq \Omega_{m,0} \leq 1$  on the horizontal axis). Here  $\Omega_{U,0} = \Omega_{k,0} = 0, \Omega_{\lambda,0} = 0, 0.05, 0.1$  (top, middle, bottom).

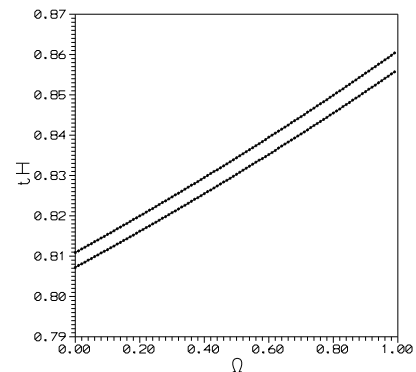


FIG. 20: The age of the universe  $t_0$  in units of  $H_0^{-1}$  for the brane models with phantom on the brane ( $0 \leq \Omega_{ph,0} \leq 1$  on the horizontal axis). Here  $\Omega_{U,0} = 0.2, \Omega_{\lambda,0} = 0.05, 0$  (top, bottom) which shows weaker influence of the brane effects to increase the age.

a dominance of the  $\rho^2$  term in the early universe. However, its admittance, even for the late universe can be dominant. In particular, if the restriction we found for dust matter on the brane from supernovae  $\Omega_{\lambda,0} \sim 0.01$  is to be applied, then the brane term can dominate the universe already at redshift  $z \sim 2$ .

For large  $z$  the brane term which comes from radiation scales like  $(1+z)^8$  and it dominates over the standard radiation term. This brings a potential trouble since in such a model radiation domination never occurs and all BBN predictions fail. In other words, the preferred value obtained from SN Ia data gives the  $\rho^2$  term which is far too large to be compatible with BBN, if we assume that brane models do not change the physics in the pre-recombination epoch.

The consistency with BBN seems to be a crucial issue in brane cosmology [49, 50, 51]. For this reason, we should admit that the contribution of brane fluid  $\Omega_{\lambda,0}$  cannot dominate over the standard radiation and dark radiation terms before the onset of BBN, i.e., for  $z \cong 10^8$

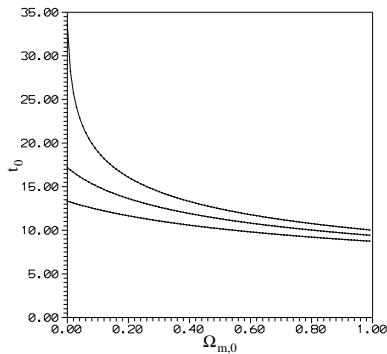


FIG. 21: The age of the universe  $t_0$  in units of  $10^9$  yrs for the flat brane model with  $\Omega_{\lambda,0} = 0, 0.004, 0.020$  (top, middle, bottom).

which gives a condition

$$\Omega_{\lambda,0} \frac{\Omega_{r,0}^2}{\Omega_{m,0}^2} (1+z)^8 < (\Omega_{r,0} + \Omega_{\mathcal{U},0}) (1+z)^4 \quad (52)$$

where  $\Omega_{\mathcal{U},0} \leq 0.11\Omega_{r,0}$  [45].

Therefore, the term

$$\Omega_{\lambda,0} \frac{\Omega_{r,0}^2}{\Omega_{m,0}^2} (1+z)^8, \quad (53)$$

which describes brane effects is constrained by the BBN because it requires a change of the expansion rate due to this term to be sufficiently small, so that an acceptable helium-4 abundance is produced. Taking this into account we obtain the following limit in this case

$$\Omega_{\lambda,0} \leq 1.0 \cdot 10^{-27} \quad \text{if } z \simeq 10^8.$$

However, the situation can significantly be changed if we admit *phantom matter* in the universe because the phantom brane term never dominates at large redshifts. Quite the contrary, it eventually dominates present and future evolution and causes no change of BBN predictions. This is because it effectively leads to a reversal of eq. (52) in a similar way as it reverses the luminosity distance relation in eq. (39).

## IX. CONCLUSIONS

We have investigated observational constraints for the Randall-Sundrum scenario of brane world cosmology. The motivation to study new observational constraints for some particular scenarios of the brane world cosmology is the demonstration that such models inspired by recent developments in the particle physics can be tested by astronomical observations.

We have shown that this scenario is compatible with the most recent observations of SN Ia. Moreover, we demonstrate that only a new (high  $z$ ) and more precise set of observations can show whether the considered class

of models constitute a viable possibility for the description of the present acceleration of the Universe.

The brane model with dust  $\gamma = 1$  matter on the brane fits the supernovae Ia data very well (including SN 1997ff at  $z \simeq 1.7$ ). However, the cosmological constant is still required. We obtain the best-fit non-flat model with  $\Omega_{\lambda,0} \simeq 0.01$ ,  $\Omega_{k,0} \simeq -0.9$ ,  $\Omega_{m,0} = 0.6$ ,  $\Omega_{\Lambda,0} = 1.3$ . For the flat model with  $\Omega_{m,0} = 0.3$  we obtain  $\Omega_{\lambda,0} = 0.004 \pm 0.016$  as a best-fit. Whereas the best-fit non-flat model is not realistic (because of large negative curvature), the flat model with the brane for the realistic value of  $\Omega_{m,0} = 0.3$  is in agreement with the SN Ia data.

On the other hand, brane models with phantom  $\gamma = -1/3$  matter on the brane also fit supernovae data and they may *mimic* the contribution from the cosmological constant which is then not required.

We have demonstrated how the values of the estimated parameters depend on the division of the sample on high and low redshifts subsamples. As a results we obtained that although the full data set (Tonry/Barris sample) of SNIa require the cosmological term, the low redshifts  $z \leq 0.25$  data set, admits decelerating model without cosmological constant. We have also demonstrated the sensitivity of results with respect to small changes of  $\mathcal{M}$  parameter.

It is interesting that brane models with dust  $\gamma = 1$  matter for high redshifts predict brighter galaxies than the Perlmutter model. Therefore, the difference between the Perlmutter model and the brane model may be detectable for high redshift  $z > 1.2$  supernovae.

Let us note that present data suggest that  $\Omega_{\lambda,0} 1.0 \simeq 10^{-2}$  but because of the large error of this estimation it is possible that  $\Omega_{\lambda,0} = 0$ . However, from future observations of supernovae at high redshift we can expect that errors in estimation of  $\Omega_{\lambda,0}$  become significantly smaller. At present the brane theory can be neither confirmed nor ruled out. In this way the future SN Ia data should allow to verify the hypothesis that  $\Omega_{\lambda,0}$  is so large as  $\Omega_{\lambda,0} \simeq 0.01$ .

We also found the other limits on the value of  $\Omega_{\lambda,0}$  from the measurements of CMB anisotropies and BBN. We obtain the strongest limits in these cases, namely  $\Omega_{\lambda,0} < 1.0 \cdot 10^{-12}$  from CMB and  $\Omega_{\lambda,0} \leq 1.0 \cdot 10^{-27}$  from BBN. However, let us note that because the errors in estimation of  $\Omega_{\lambda,0}$  from supernovae are so large the results obtained from SN Ia do not contradict those of BBN and CMB.

Of course BBN as well as CMB are very well tested areas of cosmology which do not allow for a significant deviation from the standard model and standard expansion law, except at very early times. Although consistency with BBN and CMB is a crucial issue in brane models, we must remember that in such an approach we assume that brane models does not change the physics in the pre-recombination epochs. On the other hand, the results of analysis SNIa data are independent of the physical processes in the early universe. Therefore weaker limits obtained from SNIa observations may even be more

valuable.

Research Committee (KBN) grants No 2P03B 090 23 (M.P.D.) and No 2P03B 107 22 (M.S.) is acknowledged.

## X. ACKNOWLEDGEMENTS

We wish to thank Dr. B.J. Barris for explanation the details of his SNIa sample. The support from Polish

- 
- [1] P. Hořava and E. Witten, *Nucl. Phys. B* **460** (1996), 506; *ibid* **B475**, 94.
- [2] L. Randall and R. Sundrum, *Phys. Rev. Lett.*, **83** (1999), 3370; *ibid* **83** (1999), 4690.
- [3] T. Shiromizu, K. I. Maeda, and M. Sasaki, *Phys. Rev. D* **62**, 024012 (2000).
- [4] R. Dick, *Class. Quant. Grav.* **18**, R1 (2001).
- [5] G. Dvali, G. Gabadadze, and M. Porrati, *Phys. Lett. B* **485**, 208 (2000).
- [6] C. Deffayet, *Phys. Lett. B* **502**, 199 (2001).
- [7] L. Randall, *Science* **296**, 1422 (2002).
- [8] S.-H. Henry Tye and I. Wasserman, *Phys. Rev. Lett.* **86**, 1682 (2001).
- [9] K. Koyama and J. Soda, *Phys. Rev. D* **62**, 123502 (1997).
- [10] H. Kodama, A. Ishibashi, and O. Seto, *Phys. Rev. D* **62**, 064022 (2000).
- [11] G. Dvali and G. Gabadadze, *Phys. Rev. D* **63**, 065007 (2001).
- [12] R. H. Brandenberger, D. A. Easson, and D. Kimberly, *Nucl. Phys. B* **623**, 421 (2002).
- [13] C. Deffayet, G. Dvali, and G. Gabadadze, *Phys. Rev. D* **65**, 044023 (2002).
- [14] P. M. Garnavich et al., *Astrophys. J. Lett.* **493**, L53 (1998).
- [15] S. Perlmutter et al., *Astrophys. J.* **483**, 565 (1997).
- [16] A. G. Riess et al., *Astron. J.* **116**, 1009 (1998).
- [17] B. P. Schmidt et al., *Astrophys. J.* **507**, 46 (1998).
- [18] S. Perlmutter et al., *Nature* **391**, 51 (1998).
- [19] S. Perlmutter et al., *Astrophys. J.* **517**, 565 (1999).
- [20] R.R. Caldwell, *Phys. Lett. B* **545** (2002), 23; S. Hannestad and E. Mörstell, *Phys. Rev. D* **66** (2002), 063508; P.H. Frampton, *Phys. Lett. B* **555** (2003), 139.
- [21] M.P. Dąbrowski, T. Stachowiak and M. Szydlowski, *Phys. Rev. D* **68** (2003), 103519.
- [22] A.G. Riess et al., *Ap. J.* **560** (2001), 49; *Ap. J.* **577** (2002), L1.
- [23] M. Szydlowski, M.P. Dąbrowski, and A. Krawiec, *Phys. Rev. D* **66** (2002), 064003.
- [24] M.P. Dąbrowski, *Ann. Phys (N. Y.)* **248** (1996) 199.
- [25] M.P. Dąbrowski and J. Stelmach, *Astron. Journ.* **92** (1986), 1272; *ibid* **93** (1987), 1373.
- [26] M.P. Dąbrowski and J. Stelmach, *Astron. Journ.* **97** (1989), 978.
- [27] A. Campos and C.F. Sopena, *Phys. Rev. D* **63**, 104012 (2001).
- [28] P. Singh, R.G. Vishwakarma and N. Dadhich, hep-th/0206193.
- [29] K. Freese and M. Lewis, *Phys. Lett. B* **540** (2002), 1.
- [30] K. Freese and M. Lewis, *Nucl. Phys. B (Proc. Suppl.)* **124** (2003), 50; *Ap. J.* **564** (2003), 25.
- [31] R.G. Vishwakarma et al. (astro-ph/0211285); W. Hu et al. (astro-ph/0006436).
- [32] W. Godłowski and M. Szydlowski, *GRG* **36**, 767 (2004).
- [33] Yu. Shtanov, *Phys. Lett. B* **557** (2003), 1.
- [34] P. J. E. Peebles and B. Ratra, *Rev. Mod. Phys.* **75**, 599 (2003).
- [35] R. A. Knop et al. (2003), astro-ph/0309368.
- [36] J. L. Tonry et al., *Astrophys. J.* **594**, 1 (2003), astro-ph/0305008.
- [37] B. J. Barris et al. 2003 astro-ph/0310843
- [38] B. F. Williams et al. (2003), astro-ph/0310432.
- [39] T. Padmanabhan and T. Choudhury (2002), astro-ph/0212573.
- [40] T. Choudhury and T. Padmanabhan (2003), astro-ph/0311625.
- [41] U. Alam (2003), astro-ph/0303009.
- [42] M. Doran, M. Lilley, J. Schwindt, and C. Wetterich, *Astrophys. J.* **559**, 501 (2001).
- [43] W. Hu, M. Fukugita, M. Zaldarriaga, and M. Tegmark, *Astrophys. J.* **549**, 669 (2001).
- [44] R. G. Vishwakarma P. Singh, (2002), astro-ph/0211285.
- [45] K. Ichiki, M. Yahiro, T. Kajino, M. Orito, and G. J. Mathews, *Phys. Rev. D* **66**, 043521 (2002).
- [46] P. de Bernardis et al., *Astrophys. J.* **564**, 559 (2002).
- [47] D. N. Spergel et al. (2003), astro-ph/0302209
- [48] L. Page et al. (2003), astro-ph/0302220
- [49] N. Arkani-Hamed, S. Dimopoulos, and G. Dvali, *Phys. Rev. D* **59**, 086004 (1999).
- [50] P. Binetruy, C. Deffayet, and D. Langlois, *Nucl. Phys. B* **565**, 269 (2000).
- [51] J. Bratt, A. Gault, and R. Scherrer, and T. Walker, *Phys. Lett B* **546**, 19 (2002).
- [52] <http://www.supernova.lbl.gov>, <http://snfactory.lbl.gov>.